Article **ECORFAN Journal-Taiwan**
June 2022, Vol.6 No.11 1-11

Numerical analysis of the hydrodynamic behavior of a magnetoreological fluid

Análisis numérico del comportamiento hidrodinámico de un fluido magnetoreológico

ORTEGA-ROMERO, Daysi Flor de Liz†*, ZÚÑIGA-CERROBLANCO, José Luis and HORTELANO-CAPETILLO, Juan Gregorio

Universidad Politécnica de Juventino Rosas. Master's Degree in Engineering, Mexico.

ID 1st Author: *Daysi Flor de Liz, Ortega-Romero* / **ORC ID:** 0000-0001-7364-4729, **CVU CONACYT ID:** 1198186

ID 1st Co-author: *José Luis, Zúñiga-Cerroblanco*/ **ORC ID:** 0000-0003-0493-8197

ID 2nd Co-author: *Juan Gregorio, Hortelano-Capetillo*/ **ORC ID:** 0000-0002-3702-4853

DOI: 10.35429/EJT.2022.11.6.1.11 Received January 15, 2022; Accepted June 30, 2022

Abstract

In this work, a numerical analysis of the behavior of magnetorheological fluids under the influence of different magnitudes of magnetic field is carried out. The properties of these fluids are affected and modified through the application of these magnetic fields, which has many applications in the engineering area. To carry out the analysis, a circular geometry is taken on which the magnetic field acts perpendicular to the direction of movement of the fluid. The magnetorheological fluid used is Basonetic 5030. The inlet velocity of the fluid is considered to be 1.31 m/s for the geometry of 20 and 30 mm, respectively. The Bingham viscosity model is used to obtain the viscosity. For the numerical solution is used a commercial software, in which has been used a UDF for the application of the Bingham viscosity model. Among the reported results is the velocity profile and the pressure drop along the duct for magnetic fields of 0.01 to 0.5 Teslas, here is observed the influence of the magnetic effects on the magnetorheological fluid with different diameters.

Magnetorheological fluid, Magnetic field, Computational Fluid Mechanics (CFM)

Resumen

En el presente trabajo se lleva a cabo un análisis numérico del comportamiento de fluidos magnetoreológicos bajo la influencia de diferentes magnitudes de campo magnético. Las propiedades de estos fluidos se ven afectadas y modificadas mediante la aplicación de dichos campos magnéticos, lo cual tiene diversas aplicaciones en el área de ingeniería. Para realizar el análisis, se toma una geometría de forma circular sobre la cual actúa el campo magnético perpendicular a la dirección del movimiento del fluido. El fluido magnetoreológico que se utiliza es Basonetic 5030. La velocidad de entrada del fluido se considera de 1.31 m/s para la geometría de 20 y 30 mm, respectivamente. Se utiliza el modelo de viscosidad de Bingham para la obtención de la viscosidad. Para la solución numérica se utiliza un software comercial, en el cual se ha usado un UDF para la aplicación del modelo de viscosidad Bingham. Dentro de los resultados que se reportan está el perfil de velocidad y la caída de presión a lo largo del ducto para el rango de campos magnéticos de 0.01 a 0.5 Teslas, aquí se observa la influencia de los efectos magnéticos sobre el fluido magnetoreológico con diferente diámetro.

Fluido magnetoreológico, Campo magnético, Mecánica de Fluidos Computacional (CFD)

Citation: ORTEGA-ROMERO, Daysi Flor de Liz, ZÚÑIGA-CERROBLANCO, José Luis and HORTELANO-CAPETILLO, Juan Gregorio. Numerical analysis of the hydrodynamic behavior of a magnetoreological fluid. ECORFAN Journal-Taiwan. 2022. 6-11:1-11.

* Author correspondence (E-mail: ortegadaysi06@gmail.com)
† Researcher contributing as first author.

Introduction

Magnetorheological fluids (MRFs) are dispersions of granular particles in a carrier liquid such as water, mineral oil and hydrocarbon-based oils(Çeşmeci, Ş., & Engin, 2010; Susan-Resiga, D., Bica, D., & Vékás, 2010). The particle diameter of these suspensions varies between 1 and 5 μm.

These fluids when in the absence of a magnetic field behave as a Newtonian fluid since their viscosity remains constant. However, when the fluid is exposed to a magnetic field, its properties change causing an alignment of the particles in the direction of the applied field forming chains where it acquires an increase in its viscosity, acquiring a non-Newtonian behavior and becomes a semi-solid state as can be seen in Figure 1.

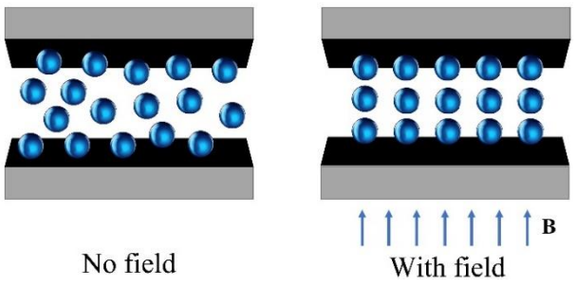

Figure 1 Formation of chains of particles suspended from an MR fluid by the presence of an external magnetic field
Source: Own elaboration

The main applications of FMRs are developed in different industrial products, i.e., from clutches, shock absorbers, valves and seals, to biomedical applications, mainly in prosthetics and cancer treatment. However, one of the disadvantages is particle sedimentation, so studies have focused on the chemical stability of these fluids.

As the viscosity of the fluid increases, the yield stress τ0 also changes. This behavior of the MR fluid corresponds to the Bingham model, as can be seen in Figure 1, which is characterized by yield stresses in relation to the intensity of the applied magnetic field. This effect is achieved because when a magnetic field is induced, the chains formed restrict the movement of the fluid, changing its rheological properties; when the field is removed, this effect disappears, returning to its initial state (Phule, 2001).

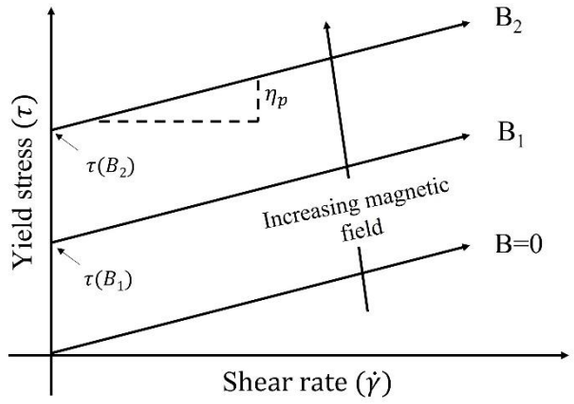

Graphic 1 Behavior of an idealized Bingham model, MR fluid in the presence of an applied magnetic field (H) as a function of shear rate
Source: Own elaboration

Background

Due to the viscous behavior of MR fluids when exposed to a magnetic field, it is possible to make devices with smaller size, but with a wide range of service (Yang, 2002), this is due to the fact that MR fluids have a facility to generate a magnetic saturation of particles.

Due to the rheological properties of MR fluids, these fluids have been implemented in several applications, mainly in the engineering area. The best known devices with MR fluids are shock absorbers that can currently be found in luxury(Bai, X-X, Chen, P, Qian, 2015; Bai, X-X, Hu, W, Wereley, 2013; Boada, MJ, Calvo, JA, Boada, BL, et, 2011; Chae, HD, Choi, 2015; Gurubasavaraju, M, Kumar, H, Mahalingam, 2018), in which there is a rapid response in controlling vibrations and oscillations resulting from walking improving vehicle stability.

ISSN 2524-2121

Research is also being conducted regarding the use of MR fluids in dampers used for building and bridge foundations (Ding, Y, Zhang, L, Zhu, H-T, et, 2013; Wu, 2010), railway suspension (Kim, H-C, Shin, Y-J, You, W, et, 2016) for the protection of these against earthquakes as it absorbs vibrations produced during these natural phenomena, they can also be found in tracked vehicles such as military and agricultural trucks (Ata, WG, Oyadiji, 2014), in the medical area have been investigated prostheses in which motors will be eliminated and therefore decreases its weight since the size of the prosthesis is reduced obtaining the same or even better performance and response time compared to other prostheses, strength is provided to the fingers or arm, in the case of leg prosthesis, it improves the walking gait, which benefits the individuals who use it, since they have a more uniform gait and therefore will not have a hip deformity as a consequence of using a prosthesis (Case, D, Taheri, B, Richer, 2014; Qiang, F, Wang, D-H, Lei, X, et, 2017), and in recent years, MR dampers were investigated to incorporate features to make it more functional, also it has attracted more interest recently in studying the damping force in MR dampers (Deng, L, Sun, S, Christie, MD, et, 2019; Huang, H, Sun, S, Chen, S, et, 2019).

Various authors have proposed several theoretical models to predict the behavior of MR fluids and each of these may be more precious than the other, however, to select one of these models should consider the mode of operation and the type of device in which it will be used.

Wang and (Liao, 2011), studied different parametric models of MR dampers, dynamic models based on Bingham, bi-viscous model and the Bouc-Wen model, upon comparison in the results obtained the Bingham dynamic model is preferred compared to the two quasi-static models due to the fact that with the dynamic model the hysteretic behavior of MR dampers can also be predicted.

Although a wide variety of rheological models have been studied to describe the behavior of MR fluids, it should be considered that the Bingham and Herschel-Bulkley models are the most widely used due to their simplicity compared to other models; however, if these two models are compared it is more appropriate to use the Herschel-Bulkley model in the case of high values in shear stress.

(Omidbeygi F, 2012) used the Herschel-Bulkley model to study the hydrodynamic characteristics of an MR fluid inside a rotational eccentric cylinder in a shear mode, results of good fluid consistency at high shear rates over a wide range of magnetic field strengths were obtained, to validate these results were compared analytically and numerically.

(Goldasz J, 2012) used the Bingham, bi-viscous and Herschel-Bulkley models to analyze the flow behavior of an MR fluid in a damper, the results obtained analytically were compared with experimental results and a good consistency and lower margin of error was obtained between the results obtained with the Herschel-Bulkley model and the experimental data.

The study of MR solutions in Poiseuille or capillary flow, there are very few works. One of them is the work of (Wang, X., & Gordaninejad, 2006) in which they performed a study of magnetorheological fluids at high shear values for three magnetorheological fluids (MRF-132LD, PAO MRPG, Ferro-MRF), with iron particles. These authors designed a viscometer where the flow was generated by the movement of a piston and in this way they controlled the speed of deformation, to store the fluid they used an accumulator and applied an external magnetic field only in a part of the channel. They found that the fluids show a non-Newtonian thinning behavior and an increase in viscosity with increasing magnetic field.

(Gedik, 2017), conducted a study comparing the results obtained experimentally and numerically of magnetorheological fluids located in a circular pipe under the influence of different magnetic field strengths, where it was shown that as the magnetic field increases the velocity decreases as the viscosity increases which results in an increase in pressure. When making the comparisons between the experimental and numerical study, the results have a variation of 6.10% when the fluid is without field and 1.71% when the field is applied, this for a 10 mm diameter pipe; however, for the 15 mm pipe a variation of the results of 2.31% without field and 0.89% when applying magnetic field was obtained. By having a very low margin of error, it shows that the results obtained from the numerical and experimental parts agree.

ISSN 2524-2121

(Pappas, Y., & Klingenberg, 2006), performed a simulation with Poiseuille geometry, i.e., of the flow of an MR fluid generated by a pressure gradient moving between two parallel magnetizable plates, the fluid is composed of dispersed particles floating in a continuous phase of Newtonian behavior, the magneto-static force was treated in the limit of the dipole point. Applying two different boundary conditions; in the first case, a no-slip and frictionless condition is considered. For this case, they found that the inclusion of friction reproduces the behavior of a Bingham fluid, which was expected to be obtained according to what was observed experimentally for MR fluids. In addition, the formation of laminar structures after the yield region was found. For the second case, the slip boundary condition produces higher flow velocities compared to the first case and thicker laminar structures, but does not reproduce the Bingham behavior, since no yield stress is present. However, for both cases the presence of velocity fluctuations is obtained. These are associated with changes in the microstructure of the fluid, where the chains are continuously broken and reformed.

One of the main advantages of using computational software for the solution of the governing equations is that the analysis can be carried out in 3D and the continuity, momentum and energy equations can be solved together.

CFD is used to simulate both laminar and turbulent fluid flows. However, there is no software that can accurately simulate a magnetorheological fluid. Therefore, existing software must be complemented, either by incorporating user-defined functions to achieve an accurate simulation of magnetorheological fluids.

In this work a numerical study of an incompressible MR fluid under a laminar regime is carried out, this fluid is conducted through a cylindrical pipe, for which a diameter of 10 and 15 mm is considered, this pipe is exposed in a section to an external and uniform magnetic field, which is applied perpendicular to the direction of flow. Computational Fluid Dynamics (CFD) analysis was used to carry out the numerical study.

Development

Geometry

Figure 2 shows the schematic representation of the pipe geometry used for the numerical analysis. Two circular geometries were made, in which, diameters of 20 and 30 mm with a length of 300 mm are considered for both cases. The flow model geometry and mesh were designed in ICEM CFD and then exported to ANSYS-Fluent for the 3D laminar flow solution.

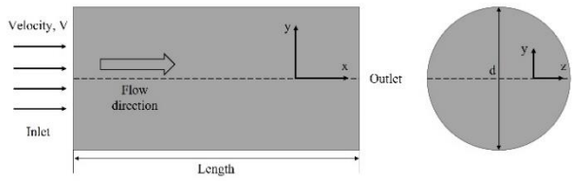

Figure 2 Schematic view of the pipe geometry used in CFD simulations
Source: Own elaboration

Materials

In this study, an MR fluid, which is Basonetic 5030, is analyzed. The MR fluid analyzed is a sample with 20% volumetric concentration of carbonyl iron powder diluted in an alpha-type polyolefin base fluid. This fluid is used for all numerical studies and its physical properties are given in Table 1. A rheometer was used to determine the viscosity of the MR fluid. As a result of the viscosity measurement, a value of 0.909 Pas was obtained at a temperature of 40°C and a shear rate of 99.55 1/s without applying a magnetic field strength.

	Basonetic 5030
Density (g/cm^3)	1.8
Viscosity (Pas, measured at 40 °C, γ=99.55 1/s)	0.909
Concentration (%)	20
Base fluid	Poly-α-olefin
Magnetizable particle	Carbonyl Iron Powder
Temperature range (°C)	-40 °C to +120 °C

Table 1 Physical properties of MR fluid
Source:(Gedik, 2017)

Mesh analysis

The generation of the geometry mesh is performed by means of a structured meshing which has as primary objective the calculation of the position of the nodes in the geometry, so that the resulting elements present certain characteristics of size and regularity, for the meshing method, a tetrahedral method is selected, with BiGeometric mesh law with variations in the number of nodes in the geometry. The information of the mesh convergence study for the 20 and 30 mm diameter pipe geometry is provided in Table 2.

Diameter (mm)	Length (mm)	Number of mesh	Number of nodes	Average speed (m/s)
10	300	1a	24000	1.0338
		2a	25780	1.3483
		3a	106600	1.1928
		4a	553200	1.4903
		5a	127200	1.6629
		6a	1279200	1.3077
		7a	223500	1.6706
		8a	302700	1.6365
		9a	444000	1.5477
		10a	739500	1.4038
		11a	952800	1.3579
		12a	1193100	1.3196
5		1b	127200	2.8359
		2b	223500	2.8438
		3b	302700	2.8323
		4b	444000	2.8032
		5b	553200	2.7597
		6b	739500	2.6594
		7b	952800	2.4705
		8b	1110000	2.1954
		9b	1279200	1.5038

Table 2 Mesh convergence information
Source: Own elaboration

In addition, the software tool chosen to mesh the model is an important decision; accuracy, flexibility and ease of use are important features to choose the most suitable one. The mesh developed for this model has been designed with the commercial software ICEM CFD, belonging to ANSYS. Figure 3 illustrates the proposed optimal mesh; it is a tetrahedral mesh with 302700 nodes, 18704 quads and 293020 hexas.

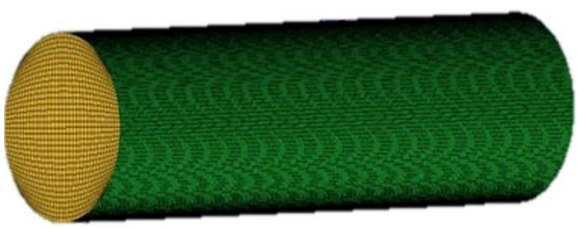

Figure 3 Optimal mallada of the geometry
Source: Own elaboration

Boundary conditions

The boundary conditions used in the simulations are: *pressure inlet* (at the duct inlet) with an inlet pressure variation of ±100 to ±500 mbar (±10000 and ±50000 Pa), *outlet vent* (duct outlet) and *wall* (for solid surfaces) which were implemented as a stationary wall and without slip conditions. These inlet conditions are taken for the study of velocities in the different cases.
As can be seen in Figure 4, the geometry is divided into three walls *WALL_1* (located 0-100 mm along the tube), *WALL_2* (located 101-200 mm along the tube) and *WALL_3* (located 201-300 mm along the tube). However, the magnetic field will only be applied in the second section, referred to as *WALL_2*.

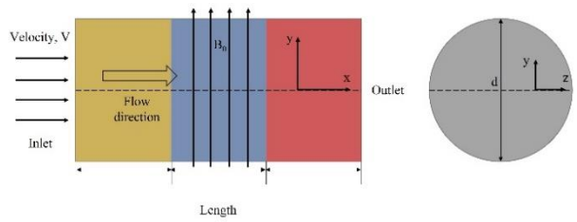

Figure 4 Boundary conditions
Source: Own elaboration

With these sections and once the velocity profiles are obtained, the boundary conditions for the implementation of the magnetic field are adjusted, which are: *velocity inlet* (at the duct inlet) where it is customized with the implementation of a UDF to define the velocity profile, *outlet vent* (duct outlet) and *wall* (for solid surfaces) which were implemented as stationary walls and without sliding conditions.

Considerations

The Herschel-Bulkley viscous model for the MR fluid is selected. Equation 1 representing this model is presented below:

$$\tau = \tau_0 + K(\gamma)^n \quad (1)$$

Where *K* indicates the consistency index (kg/ms), n the power law index, τ_0 the initial shear stress (Pa), γ the critical shear rate (1/s).
However, to carry out the calculation of the initial shear stress, it is performed by Equation 2, this stress is calculated in relation to the applied magnetic field.

$$\tau_0(H) = \mathrm{C} \cdot 2.717 \times 10^5 \cdot \Psi^{1.5239} \tanh\left(6.33 \times 10^{-6} H\right) \quad (2)$$

where τ_0 indicates the initial shear stress (Pa), C is a constant, Ψ is the volume fraction and H is the magnetic field strength (Teslas).

Governing equations

The equations of continuity of mass and momentum of steady motion of an incompressible MR fluid under a magnetic field in a cylindrical pipe are:

$$\nabla . V = 0 \tag{3}$$

$$\rho \frac{DV}{Dt} = -\nabla P + \mu \Delta V + F_m \tag{4}$$

where ∇P denotes the pressure gradient (Pa/m), ρ the fluid density (kg/m^3) and μ the dynamic viscosity of the fluid (kg/ms) and F_m is the electromagnetic force which can be expressed as follows:

$$F_m = \eta(J \times H) = J \times B \tag{5}$$

Where J indicates the intensity of the electric current expressed below according to Ohm's law:

$$J=\sigma(E+V\times B) \tag{6}$$

Where σ indicates the electrical conductivity of the fluid, E the magnitude of the electric field, V the average flow velocity vector and B is the magnetic field induction.

Results

However, these meshes present problems when converging and have high variations in the velocity results along the pipe, these variations are from 0.5 to 3 m/s, which indicates that these meshes are not optimal to use since the values are very variable and the results obtained will be very unreliable, these results are shown in Figure 2.

Having a deficient mesh, which does not comply with the necessary standards, can dramatically alter its characteristics and as a consequence have very unreliable results since they will not represent the expected phenomena.

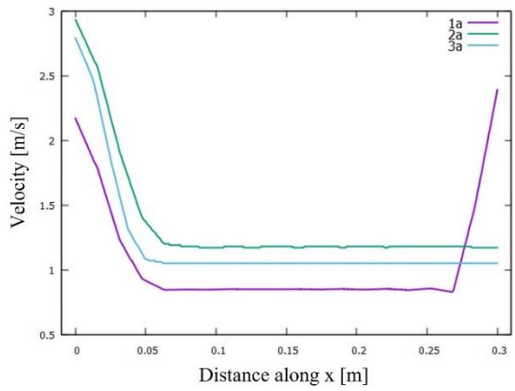

Graphic 2 Mesh convergence study for d=20mm, non-convergent
Source: Own elaboration

As can be clearly seen in Graph 3 and 4 for diameters of 20 and 30 mm, respectively, the smaller the size of the separation between the mesh nodes, i.e., the higher the mesh density, the higher the velocities, and after a certain mesh size, no significant change in velocities is observed. The information from the mesh convergence study for the pipe geometries is broken down in Table 2.

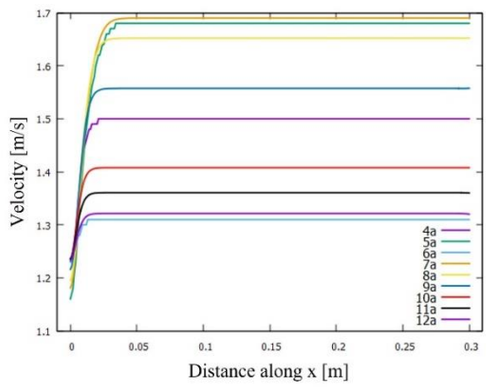

Graphic 3 Mesh convergence study for d=20mm, convergent
Source: Own elaboration

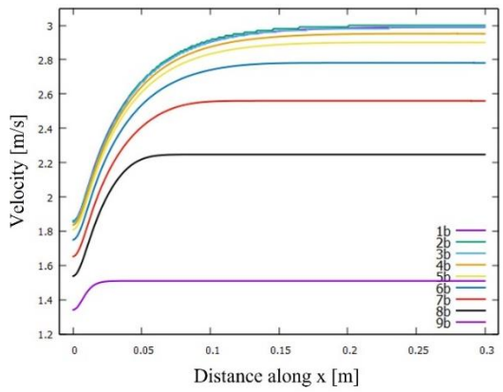

Figure 4 Mesh convergence study for d=30mm, convergent
Source: Own elaboration

The axial velocity profiles were plotted in Figure 5 with and without applied magnetic field. As can be clearly seen in the graph, the velocity value is 1.27 m/s for the situation when B = 0 Teslas, this for the Basonetic 5030 fluid in a 20 mm pipe, decreasing the velocity according to the increase of the magnetic field strength. As a result of these increases, flow velocity values of 1.16, 1.12, 1.02 and 0.983 m/s were found for magnetic field B = 0.06, 0.1, 0.3 and 0.5 Teslas, respectively.

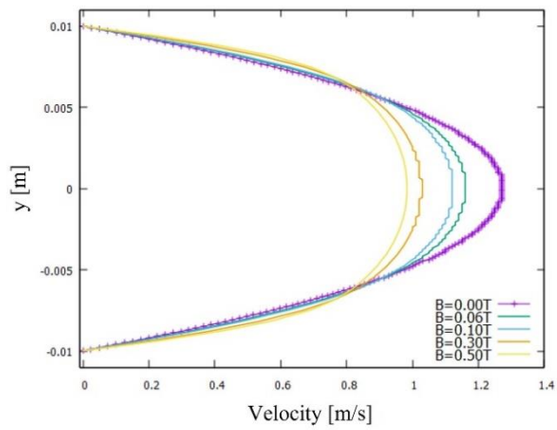

Graphic 5 Variations of velocity profiles as a function of increasing magnetic field, for d=20 mm, BASONETIC 5030
Source: Own elaboration

Similarly, these values turned out to be 1.23, 1.20, 1.03 and 0.995 m/s with the same increasing values of B for the pipe diameter of 30 mm while it was 1.30 m/s for the situation B = 0 Teslas as can be observed in Graphic 6.

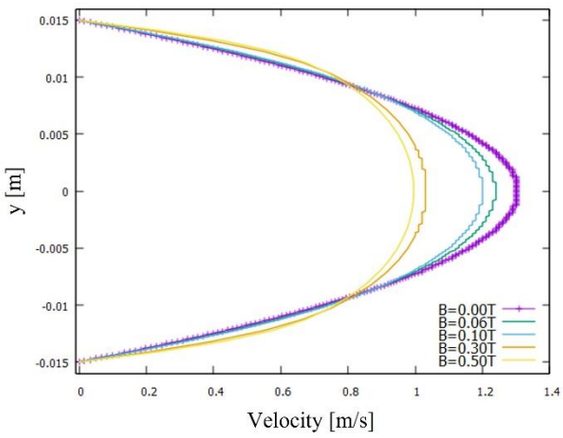

Graphic 6 Variations of velocity profiles as a function of increasing magnetic field, for d=30 mm, BASONETIC 5030
Source: Own elaboration

The increase in magnetic field strength has caused the decrease in flow velocities for all MR fluids and the decrease in pipe diameter increases the flow velocity and pressure as expected.

In graphics7 and 8, the numerical velocity vectors of the pipe having 20 and 30 mm diameter for Basonetic 5030 fluid are shown, respectively. It is clear from the figure that the externally applied magnetic field in the *WALL_2* section has caused the velocity of the MR fluid flowing inside the pipe to decrease, since, when a magnetic field is applied, the particles tend to polarize and align with the field, decreasing the distance between molecules and, consequently, the resistance of the molecules to move increases. Thus, the viscosity of these fluids increases as a function of the intensity of the applied field.

When B = 0 Teslas the value of the velocity is equal to 1.27 m/s and the fluid flow results in smaller flow rates in situations B ≠ 0 Teslas compared to the situation where there is absence of magnetic field strength. At zero and low magnetic field values, the axial velocity profile is parabolic and as B increases, the profiles decrease maintaining the parabolic profile, as can be seen in Figure 5.

ISSN 2524-2121

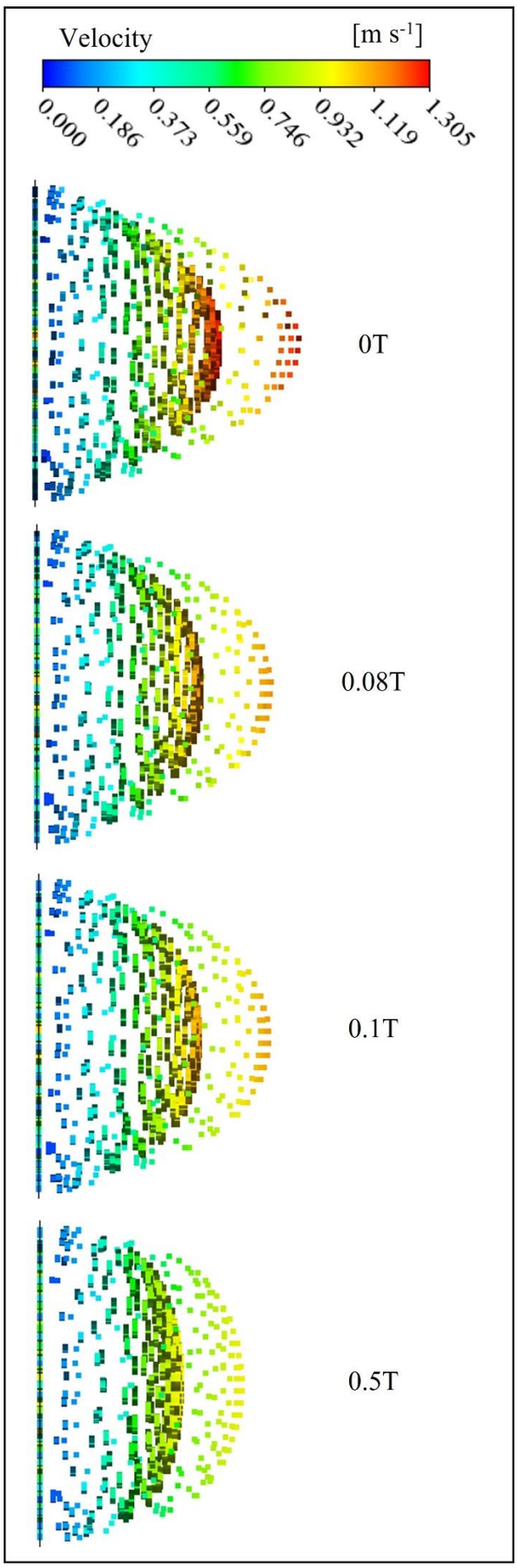

Graphic 7 Magnitude of velocity under different magnetic field strengths, d=20mm, BASONETIC 5030
Source: Own elaboration

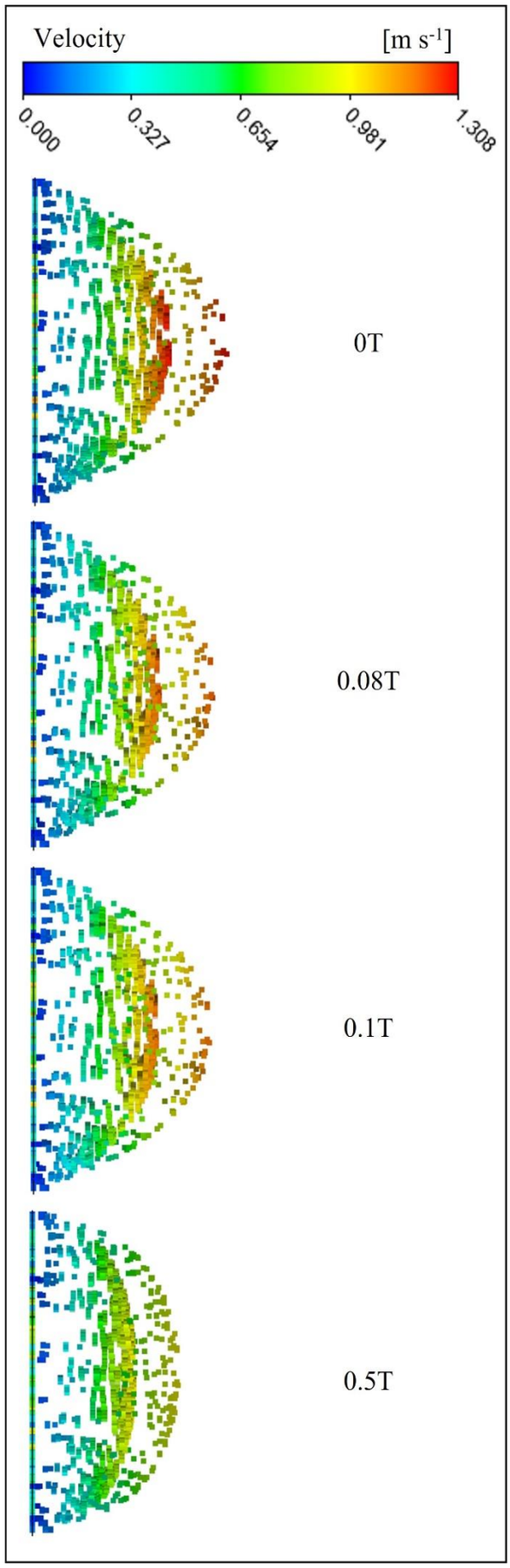

Graphic 8 Magnitude of velocity under different magnetic field strengths, d=30mm, BASONETIC 5030
Source: Own elaboration

ISSN 2524-2121

This effect is obtained because when a particle is positioned perpendicularly in a uniform magnetic field, it begins to experience a force that will force it to change the direction of its velocity vector, causing it to move in a uniform circular motion.

The pressure differences measured in the numerical study and the velocity variations within the center of the pipe depend on the increase of the magnetic field strength.

In Graphic 9 it can be clearly seen, when the magnetic field increases, the pressure values increase. The pressure values obtained as 0.779 and 0.335 kPa in the situation of no applied magnetic field (B = 0 Teslas) for the fluid in the 20 and 30 mm pipes, respectively, have increased in the presence of the magnetic field and these values have gone to 2.720 and 1.588 kPa, respectively, for the value of the magnetic field B = 0.5 Teslas.

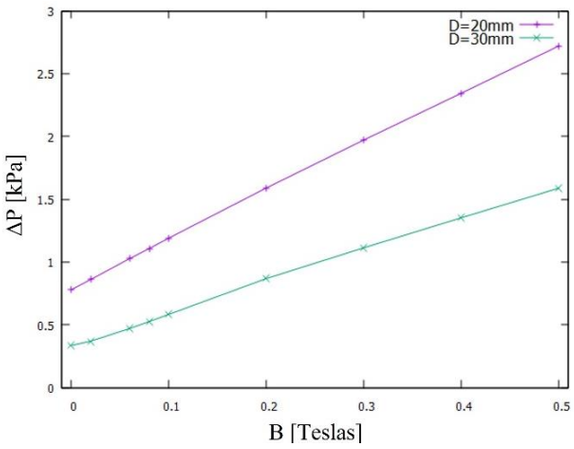

Graphic 9 Pressure variations as a function of increasing magnetic field strength
Source: Own elaboration

Conclusions

In this study, the laminar flow of a viscous and incompressible MR fluid was examined numerically. A CFD tool was used for the numerical study. The numerical study was performed using magnetic fields perpendicular to the flow of B = 0, 0.02, 0.06, 0.08, 0.1, 0.2, 0.3, 0.4 and 0.5 Teslas.

The fluid flow under the influence of the pressure gradient $\partial P/\partial x$ is in the x direction. Analyses were performed and compared for two different MR fluid flow models, the first being Newtonian (no magnetic field) and non-Newtonian (under magnetic field).

In the simulations, axial velocity values of 1.27 and 1.30 m/s have been found for Basonetic 5030 fluid for 20 and 30 mm pipe, respectively, when B = 0 Teslas.

It has been observed that the velocities and flow rates have increased with the decrease of the pipe diameter, considering that it is an incompressible fluid with stationary flow, the velocity in a conduit is inversely proportional to the surface area, since when the fluid is introduced in a region with smaller diameter, being smaller area, the velocity should be higher, but according to Bernoulli's equation, if the velocity increases, the pressure should decrease.

Regarding the results when the viscous model is adjusted, the increase of the magnetic field results in profiles with lower velocity, because as the magnetic field increases the fluid particles align in the direction of the field with higher velocity and consequently directly affects the viscosity of the fluid since the distance between the particles is smaller and therefore the resistance to flow is greater, due to the increase of this resistance as a function of the magnetic field, the pressure is affected; That is to say, the pressure increases with respect to the increase of the intensity of the magnetic field, since the smaller the distance between the particles, the more force is needed to move them. However, it is shown that the effect of the magnetic field is present in the simulation with the expected behavior.

It should be noted that the CFD simulation described in this work may represent a useful starting point to investigate more complex problems, such as non-stationary flows, more complex geometries or boundary conditions where slip is taken into account.

ISSN 2524-2121

Nomenclature

ρ	Density (g/cm^3)
μ	Viscosity (Pa•s)
τ	Shear stress (Pa)
$\dot{\gamma}$	Critical shear rate (1/s)
σ	Electrical conductivity (μmho/cm)
ΔP	Pressure difference (Pa)
H	Magnetic field strength (Tesla)
d	Diameter (mm)
E	Magnitude of the electric field (V/m)
F_m	Electromagnetic force (Tesla)
J	Electrical current intensity (Amperio)
k	Consistency index (kg/m•s)
MR	Magnetorheological
N	Pressure gradient (Pa/m)
n	Energy law index
P	Pressure (Pa)
V	Velocity (m/s)
x	Axial coordinate
y	Radial coordinate
z	Tangential coordinate

References

Ata, WG, Oyadiji, S. (2014). An investigation into the effect of suspension configurations on the performance of tracked vehicles traversing bump terrains. *Vehicle System Dynamics*, *52 (7)*, 969–991. https://doi.org/10.1080/00423114.2014.909943

Bai, X-X, Chen, P, Qian, L.-J. (2015). Principle and validation of modified hysteretic models for magnetorheological dampers. *Smart Materials and Structures*, *24 (8)*, 085014. https://doi.org/10.1088/0964-1726/24/8/085014

Bai, X-X, Hu, W, Wereley, N. (2013). Magnetorheological Damper Utilizing an Inner Bypass for Ground Vehicle Suspensions. *IEEE Transactions on Magnetics*, *49 (7)*, 3422–3425. https://doi.org/10.1109/TMAG.2013.2241402

Boada, MJ, Calvo, JA, Boada, BL, et, A. (2011). Modeling of a magnetorheological damper by recursive lazy learning. *International Journal of Non-Linear Mechanics*, *46 (3)*, 479–485. https://doi.org/10.1016/j.ijnonlinmec.2008.11.019

Case, D, Taheri, B, Richer, E. (2014). Dynamical Modeling and Experimental Study of a Small-Scale Magnetorheological Damper. *IEEE/ASME Transactions on Mechatronics*, *19 (3)*, 1015–1024. https://doi.org/10.1109/TMECH.2013.2265701

Çeşmeci, Ş., & Engin, T. (2010). Modeling and testing of a field-controllable magnetorheological fluid damper. *International Journal of Mechanical Sciences*, *52*, 1036–1046. https://doi.org/10.1016/j.ijmecsci.2010.04.007

Chae, HD, Choi, S.-B. (2015). A new vibration isolation bed stage with magnetorheological dampers for ambulance vehicles. *Smart Materials and Structures*, *24 (1)*, 017001. https://doi.org/10.1088/0964-1726/24/1/017001

Deng, L, Sun, S, Christie, MD, et, A. (2019). Experimental testing and modelling of a rotary variable stiffness and damping shock absorber using magnetorheological technology. *Journal of Intelligent Material Systems and Structures*, *30 (10)*, 1453–1465. https://doi.org/10.1177/1045389X19835955

Ding, Y, Zhang, L, Zhu, H-T, et, A. (2013). A new magnetorheological damper for seismic control. *Smart Materials and Structures*, *22 (11)*, 115003. https://doi.org/10.1088/0964-1726/22/11/115003

Gedik, E. (2017). Experimental investigation of magnetohydrodynamic flow in cıcrcular pipes and numerical analysis wıth computational fluid dynamics. *Journal of Applied Fluid Mechanics*, *10*, 801–811. https://doi.org/10.18869/acadpub.jafm.73.240.26830

Goldasz J, S. B. (2012). Nondimensional characterization of flow-mode magnetorheological/electrorheological fluid dampers. *Journal of Intelligent Material Systems and Structures*, *23*, 1545–1562.

Gurubasavaraju, M, Kumar, H, Mahalingam, A. (2018). An approach for characterizing twin-tube shear-mode magnetorheological damper through coupled FE and CFD analysis. *Journal of the Brazilian Society of Mechanical Sciences and Engineering*, *40 (3)*, 1–14. https://doi.org/10.1007/S40430-018-1066-Z

Huang, H, Sun, S, Chen, S, et, A. (2019). Numerical and experimental studies on a new variable stiffness and damping magnetorheological fluid damper. *Journal of Intelligent Material Systems and Structures*, *30 (11)*, 1639–1652. https://doi.org/10.1177/1045389X19844003

ISSN 2524-2121

Kim, H-C, Shin, Y-J, You, W, et, A. (2016). A ride quality evaluation of a semi-active railway vehicle suspension system with MR damper: Railway field tests. Proceedings of the Institution of Mechanical Engineers, Part F. *Journal of Rail and Rapid Transit*, *231 (3)*, 306–316. https://doi.org/10.1177/0954409716629706

Liao, D. H. W. and W. H. (2011). Magnetorheological Fluid Dampers: A Review of Parametric Modelling. *Smart Materials and Structures*, *20*, 01–34. https://doi.org/10.1088/0964-1726/20/2/023001

Omidbeygi F, H. S. (2012). Experimental study and CFD simulation of rotational eccentric cylinder in a magnetorheological fluid. *Journal of Magnetism and Magnetic Materials*, *324*, 2062–2069. https://doi.org/10.1016/j.jmmm.2012.02.016

Pappas, Y., & Klingenberg, D. J. (2006). Simulations of magnetorheological suspensions in Poiseuille flow. *Rheologica Acta*, *45*, 621–629. https://doi.org/https://doi.org/10.1007/s00397-005-0016-8

Phule, P. P. (2001). Magnetorheological (MR) fluids: principles and applications. *Smart Materials Bulletin*, *2001*(Elsevier), 7–10.

Qiang, F, Wang, D-H, Lei, X, et, A. (2017). A magnetorheological damper-based prosthetic knee (MRPK) and sliding mode tracking control method for an MRPK-based lower limb prosthesis. *Smart Materials and Structures*, *26 (4)*, 045030. https://doi.org/10.1088/1361-665X/aa61f1

Susan-Resiga, D., Bica, D., & Vékás, L. (2010). Flow behaviour of extremely bidisperse magnetizable fluids. *Journal of Magnetism and Magnetic Materials*, *322*, 3166–3172. https://doi.org/10.1016/j.jmmm.2010.05.055

Wang, X., & Gordaninejad, F. (2006). Study of magnetorheological fluids at high shear rates. *Rheologica Acta*, *45*, 899–908. https://doi.org/https://doi.org/10.1007/s00397-005-0058-y

Wu, B. (2010). CFD simulation of gas and non-Newtonian fluid two-phase flow in anaerobic digesters. *Water Research*, *44 (13)*, 3861–3874. https://doi.org/10.1016/j.watres.2010.04.043

Yang, G. (2002). *Large-scale magnetorheological fluid damper for vibration mitigation: modeling, testing and control*. http://sstl.cee.illinois.edu/papers/gyang2_thesis.pdf

ISSN 2524-2121